

# High-Speed Nanoindentation Mapping of Additive Manufactured Titanium Alloys for Aerospace Application

Zhiying Liu<sup>1</sup>, Haoxiu Chen<sup>1</sup>, and Yu Zou<sup>1</sup> (✉)

<sup>1</sup> Department of Materials Science & Engineering, Faculty of Applied Science & Engineering, University of Toronto, Toronto, ON, Canada  
[mse.zou@utoronto.ca](mailto:mse.zou@utoronto.ca)

**Abstract.** High-speed nanoindentation mapping was carried out using a nanoindenter (iMicro, KLA Tencor, USA) using the method of Nanoblitz3D. This method enables generating high-resolution spatial  $H$  and  $E$  maps over large areas (up to hundreds of microns) by performing up to thousands of indents. Each indent test took up to 1 second, including the surface approaching, loading, unloading, retracting, and positioning the sample for the next test. A diamond Berkovich tip (Synton-MDP, Switzerland) was used for the nanoindentation tests. Several trial-and-error nanoindentation experiments were conducted to identify an optimal indentation depth and indent spacing. In our study, we performed the indentation mapping to capture the intrinsic  $H$  and  $E$  of the  $\alpha$  and  $\beta$  phases in a Ti-6Al-2Zr-V-Mo alloy. The ratio of indent spacing to indentation depth is larger than 10 to avoid any overlapping effect between indentations. A maximum load of 1 mN, which results in a penetration depth ranging between 50 and 100 nm for  $\alpha$  and  $\beta$  grains, and 500 nm spacing between the indents were chosen for all the tests. The  $H$  and  $E$  of  $\alpha$  and  $\beta$  phases in the as-deposited and heat-treated samples are obtained from the same load, which are valid for comparison. The nanoindentation mapping with  $\sim 10,000$  indents ( $50 \times 50 \mu\text{m}^2$  areas) and  $\sim 20,000$  indents ( $50 \times 100 \mu\text{m}^2$  area) were carried out on the as-deposited and heat-treated samples, respectively. The indented areas of both samples contain more than 10  $\alpha$  and  $\beta$  grains to obtain microstructure-property correlations. The hardness ( $H$ ) and reduced elastic modulus ( $E_r$ ) at each test location can be calculated using the standard Oliver and Pharr method. The  $E_r$  includes the elastic contributions of both the indenter and the indented materials.

**Keywords:** Additive manufacturing · Titanium alloys · Nanomechanics

## 1 High-Speed Nanoindentation Mapping

High-speed nanoindentation mapping was carried out using a nanoindenter (iMicro, KLA Tencor, USA) using the method of Nanoblitz3D. This method enables generating high-resolution spatial  $H$  and  $E$  maps over large areas (up to hundreds of microns) by performing up to thousands of indents. Each indent test took up to 1 second, including the surface approaching, loading, unloading, retracting, and positioning the sample for the next test. A diamond Berkovich tip (Synton-MDP, Switzerland) was used for the

nanindentation tests. Several trial-and-error nanindentation experiments were conducted to identify an optimal indentation depth and indent spacing. In our study, the indentation depth should be more than 50 nm to capture the intrinsic  $H$  and  $E$  of the  $\alpha$  and  $\beta$  phases, while the ratio of indent spacing to indentation depth should be larger than 10 to avoid any overlapping effect between indentations [1]. A maximum load of 1 mN, which results in a penetration depth ranging between 50 and 100 nm for  $\alpha$  and  $\beta$  grains, and 500 nm spacing between the indents were chosen for all the tests. The  $H$  and  $E$  of  $\alpha$  and  $\beta$  phases in the as-deposited and heat-treated samples are obtained from the same load, which are valid for comparison. The nanindentation mapping with  $\sim 10,000$  indents ( $50 \times 50 \mu\text{m}^2$  areas) and  $\sim 20,000$  indents ( $50 \times 100 \mu\text{m}^2$  area) were carried out on the as-deposited and heat-treated Ti-6Al-2Zr-V-Mo (TA15) samples [2], respectively. The indented areas of both samples contain more than 10  $\alpha$  and  $\beta$  grains to obtain microstructure-property correlations. The selected microstructures and resulted micromechanical properties of both samples are representative. The hardness ( $H$ ) and reduced elastic modulus ( $E_r$ ) at each test location can be calculated using the standard Oliver and Pharr method [3]. The  $E_r$  includes the elastic contributions of both the indenter and the indented materials, as expressed by the following equation:

$$\frac{1}{E_r} = \frac{(1-\nu^2)}{E} + \frac{(1-\nu'^2)}{E'} \quad (1)$$

where  $E'$  (1141 GPa) and  $\nu'$  (0.07) are the elastic modulus and Poisson's ratio of the diamond Berkovich indenter, respectively. The Poisson's ratio  $\nu$  of the TA15 alloy is  $\sim 0.39$  [2]. Because the calculated  $E$  is about 98% of the  $E_r$  in this work, the  $E_r$  is used in this work to approximately represent the  $E$  of the TA15 alloys.

## 2 Microstructure Characterization

The microstructures and nanindentation impressions of both as-deposited and heat-treated samples were imaged using a scanning electron microscope (SEM, Hitachi 3500, Japan) equipped with a backscattered electron (BSE) detector. Phases in the as-deposited and heat-treated samples were determined by X-ray diffraction (XRD, Rigaku MiniFlex 600) over a  $2\theta$  range between  $30^\circ$  and  $90^\circ$  at a scanning rate of  $0.025^\circ \text{ s}^{-1}$ . The quantitative chemical compositions of  $\alpha$  and  $\beta$  phases and the element maps were acquired using an electron probe microanalyzer (EMPA, JEOL JXA8230).

## 3 Results and Discussion

Figure 1a shows a schematic of the Laser Melting Deposition (LMD) process, and Fig. 1b, c present the high-speed nanindentation mapping process and nanindentation impressions, respectively. Prior to the nanindentation tests, we characterized the

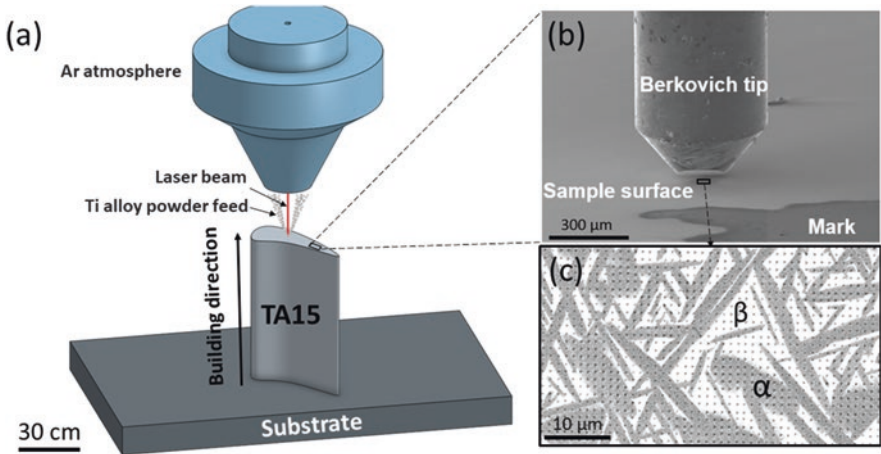


**Fig. 1.** (a) A schematic of the LMD system for additive manufacturing of the titanium alloy (TA15). (b) The SEM image of the nanoindenter with the Berkovich tip on the titanium sample surface. (c) The BSE image revealing the nanoindentation impressions on the  $\alpha$  and  $\beta$  phases of the TA15 sample after the high-speed nanoindentation mapping.

pre-indent regions using Electron Probe Microanalyzer (EPMA) to elucidate the contribution of chemical composition to the resulting  $H$  and  $E$  values of  $\alpha$  and  $\beta$  grains.

Figure 2 shows the microstructure, the corresponding  $H$  and  $E$  maps of the as-deposited TA15 sample [4]. The majority of the  $\alpha$  grains, far larger than the  $\beta$  grains, can be captured and correlated with the spatial  $H$  and  $E$  maps (Figs 2a, b and d). For example, the three  $\alpha$  grains, intersected by the line AB in Fig. 2a, involve tens of indents, showing the profile in the  $H$  and  $E$  maps. We can accurately extract the  $H$  and  $E$  values along with the line AB by point-to-point analysis, as shown in Fig. 2c. The  $\alpha$  grains show distinct  $H$  and  $E$  values. High-resolution  $H$  and  $E$  maps also virtualize the morphology of the  $\alpha$  and  $\beta$  grains, including a clear profile of the  $\alpha/\beta$  boundaries. It is believed  $\alpha/\beta$  boundaries are critical to determine the local deformation mechanism. Here, the high-speed nanoindentation mapping enables to measure the  $H$  and  $E$  distribution in the vicinity of the  $\alpha/\beta$  boundary. It should be noted the effect of the  $\alpha/\beta$  boundary on the  $H$  and  $E$  characterization is neglectable according to the absence of  $H$  or  $E$  change when approaching  $\alpha/\beta$  boundaries (Fig. 2). Figure 3 presents the microstructure, corresponding  $H$  and  $E$  maps, and Al content of the heat-treated TA15 sample. The excellent correlation between the microstructure and mechanical property maps ( $H$  and  $E$ ) is attributed to the large size of  $\alpha$  and  $\beta$  grains. The contrasting  $H$  and  $E$  in the  $\alpha+\beta$  microstructure are clearly observed. The  $\alpha$  grains exhibit distinct  $H$  and  $E$ , which is consistent with the observation in the as-deposited sample. The homogeneous Al distribution in the  $\alpha$  grains excludes the contribution of the solid solution strengthening to the contrasting  $H$  and  $E$  of the  $\alpha$  grains. The  $H$  and  $E$  contrasts in the  $\alpha$  grains should stem from the anisotropy of the hcp crystal structure. In addition to the titanium alloy, high speed nanoindentation mapping tests can be also used to capture grain-sclae mechanical properties in other multiple phase alloys, *e.g.*, graded  $\gamma$ -TiAl/Ti2AlNb alloys [5] and steel [6].

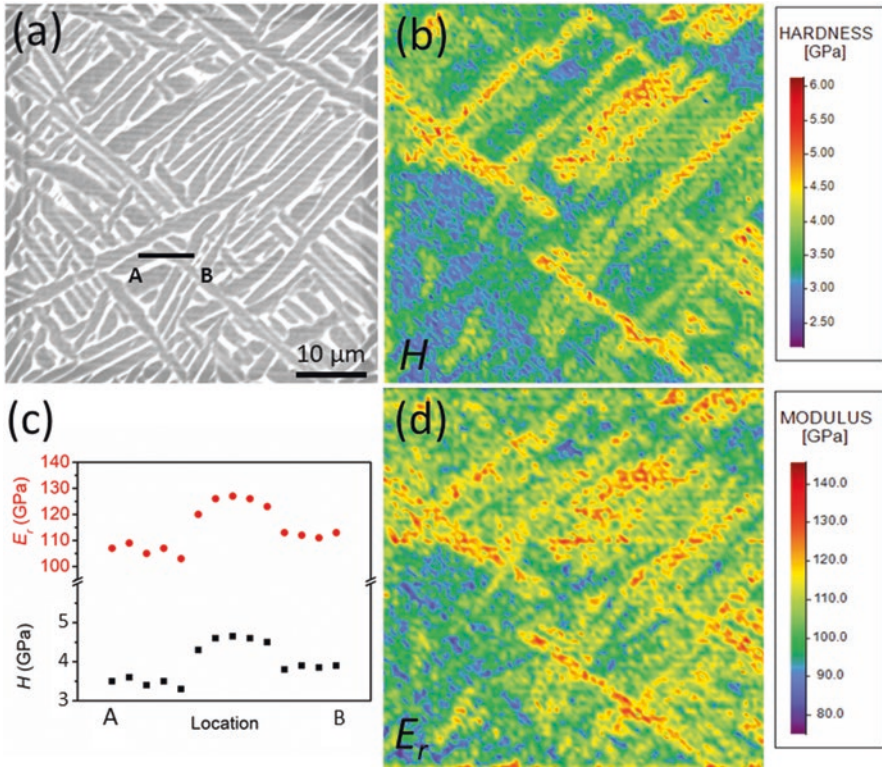


**Fig.2.** (a) BSE image of the as-deposited TA15 alloy. (b) The hardness ( $H$ ) and (d) elastic modulus ( $E$ ) of the rectangle region in (a). (c) The  $H$  and  $E$  values along with the line AB in 3(a), which involves three  $\alpha$  grains.

### 4 Conclusions

In this study, we employ the high-speed nanoindentation technique to characterize the local mechanical properties (hardness and Young’s modulus) of a near- $\alpha$  titanium alloy, Ti-6Al-2Zr-Mo-V or TA15, made by laser melting deposition. The following conclusions are drawn:

1. The high-speed nanoindentation mapping is an effective approach to reveal mechanical contrasts ( $H$  and  $E$ ) of multiphase alloys with complex microstructures, such as 3D printed titanium alloys. The speed of indentation can reach approximately 1 second per indent (10,000 indents for ~2.5 hours). The special resolution can reach the submicrometer regime (~300–500 nm). For the heat-treated TA15 sample, this method provides the  $H$  and  $E$  distributions, clearly correlates the dual-phase ( $\alpha + \beta$ ) microstructure, reveals the anisotropy of the hcp  $\alpha$  phase. This method shows a limited mechanical-phase correlation for the as-deposited sample due to its ultrafine microstructure (grain size ~ 1  $\mu$ m).



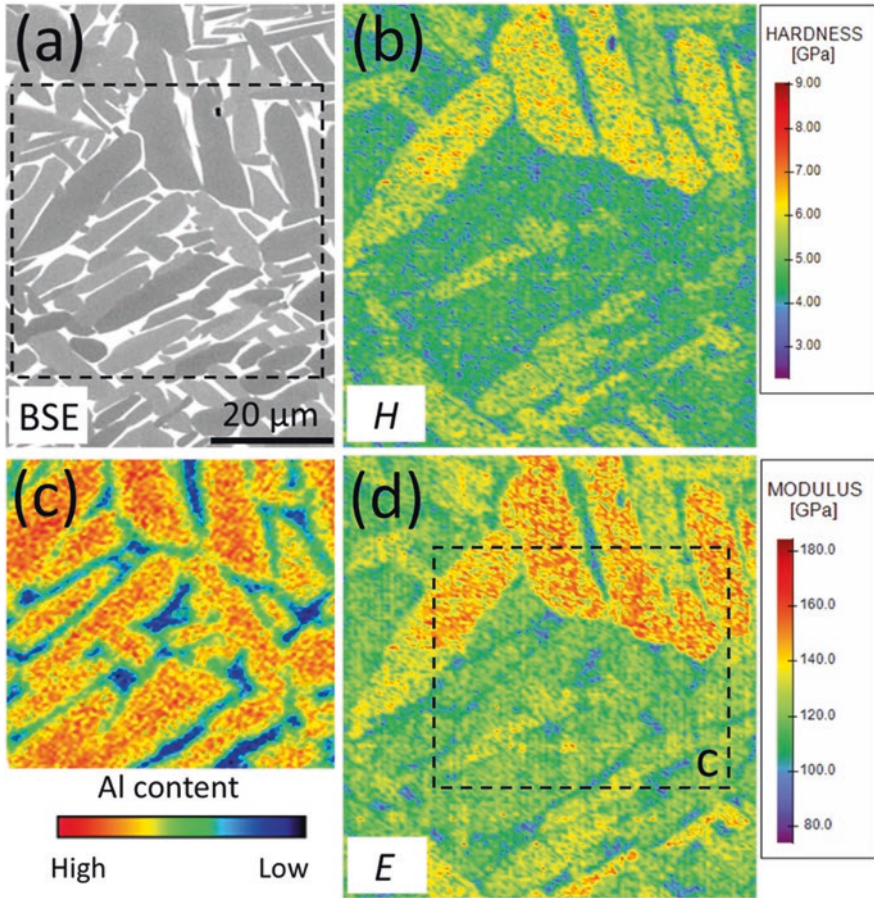


**Fig. 3.** (a) BSE image of the heat-treated TA15 alloy. (b) The  $H$  and (d)  $E$  maps of the rectangle region in 3(a). (c) The distribution of Al content in the rectangle region in 3(d), as measured by EPMA.

- Using such a method, we observe that heat treatment leads to a concurrent hardening of the  $\alpha$  and  $\beta$  phases, increasing by 32% and 12%, respectively. This phenomenon is associated with the redistribution of alloying elements: Al diffuses from the  $\beta$  phase into neighboring  $\alpha$  phase, while Mo and V diffused along the opposite direction. The element redistribution also results in the increment of the  $E$ , by 4% in the  $\beta$  phase and 14% in the  $\alpha$  phase. This mechanical distribution cannot be easily revealed using conventional indentation methods.
- Toward broad applications, the high-speed nanoindentation technique, together with advanced microstructure characterization and machine learning tools, brings unique opportunities to study and design new multiphase materials across length scales.

## References

1. Phani PS, Oliver W. A critical assessment of the effect of indentation spacing on the measurement of hardness and modulus using instrumented indentation testing. *Mater Des.* 2019;164:107563.
2. Liu Z, He B, Lyu T, Zou Y. A review on additive manufacturing of titanium alloys for aerospace applications: directed energy deposition and beyond Ti-6Al-4V. *JOM.* 2021;73:1804–18.
3. Oliver W, Pharr G. Nanoindentation in materials research: Past, present, and future. *MRS Bulletin.* 2010;35(11):897–907.
4. Liu Z, Zhang J, He B, Zou Y. High-speed nanoindentation mapping of a near-alpha titanium alloy made by additive manufacturing. *J Mater Res.* 2021;36(4):2223–34.
5. Chen H, Liu Z, Cheng X, Zou Y. Laser deposition of graded  $\gamma$ -TiAl/Ti<sub>2</sub>AlNb alloys: microstructure and nanomechanical characterization of the transition zone. *J. Alloys Compd.* 2021;875:159946.
6. Chen H, Niu G, Wu H, Zou Y. Revealing non-uniform work-hardening in a heterogeneous structured steel using high-speed nanoindentation. *JOM.* 2022;74(6):2238–44.